Supplemental Information

Enhanced Optical Transmission Mediated by Localized Plasmons in Anisotropic, 3D Nanohole Arrays

Jiun-Chan Yang†, Hanwei Gao†, Jae Yong Suh†, Wei Zhou‡, Min Hyung Lee†, and

*Teri W. Odom†‡**

† Department of Chemistry, ‡ Department of Materials Science and Engineering

Northwestern University, Evanston, IL 60208, USA

* To whom correspondence should be addressed. Email: todom@northwestern.edu

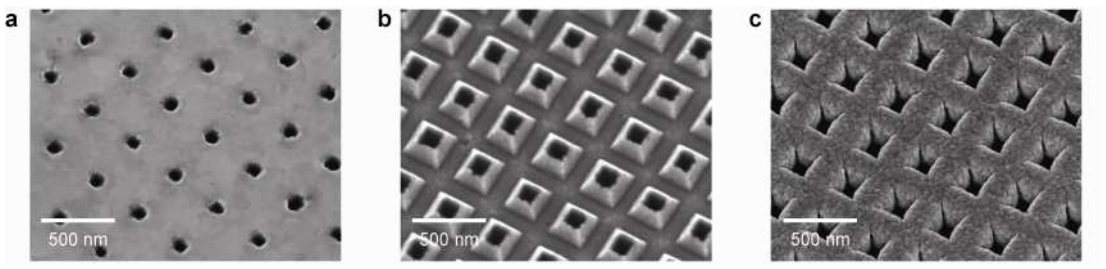

Figure S1. Surface geometry of three types of hole arrays with 100-nm openings. (**a**) Planar, (**b**) protruding, and (**c**) recessed hole arrays. The tilt angle of SEM images was 30°. Hole-hole spacing was 400 nm.

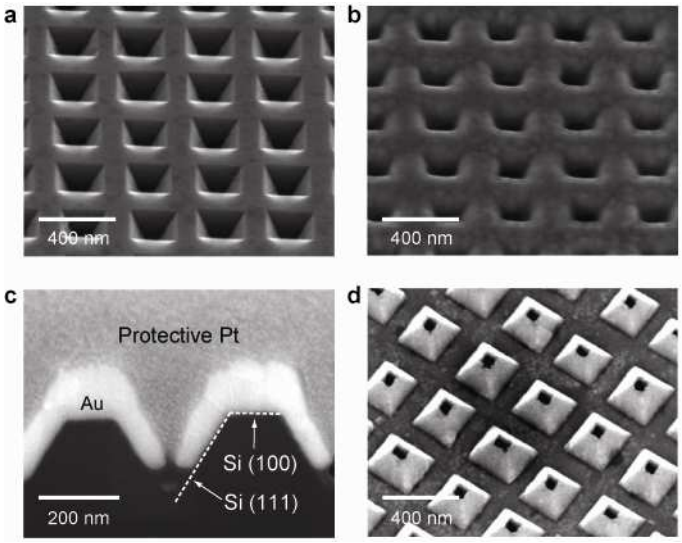

Figure S2. Surface geometry of protruding hole arrays with 50-nm openings. (**a**) Si template fabricated by SIL followed by PEEL (Methods). (**b**) Si template after depositing Au at $\alpha = 45°$, a smaller angle than that in Fig. 1. (**c**) FIB cross-section of Fig. S2b. (**d**) 3D protruding hole array with hole size = 50 nm.

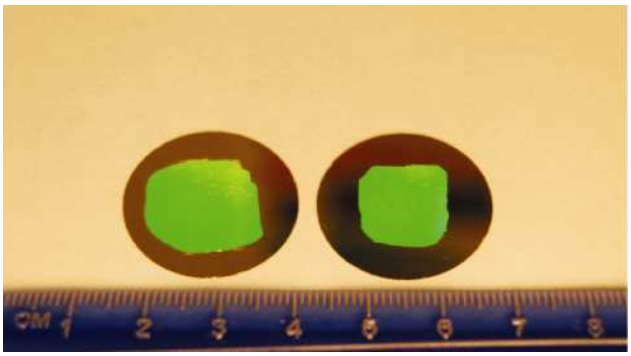

Figure S3. 3D nanohole arrays with samples areas > 1 cm^2. The optical photograph of 3D nanohole arrays on glass coverslips.

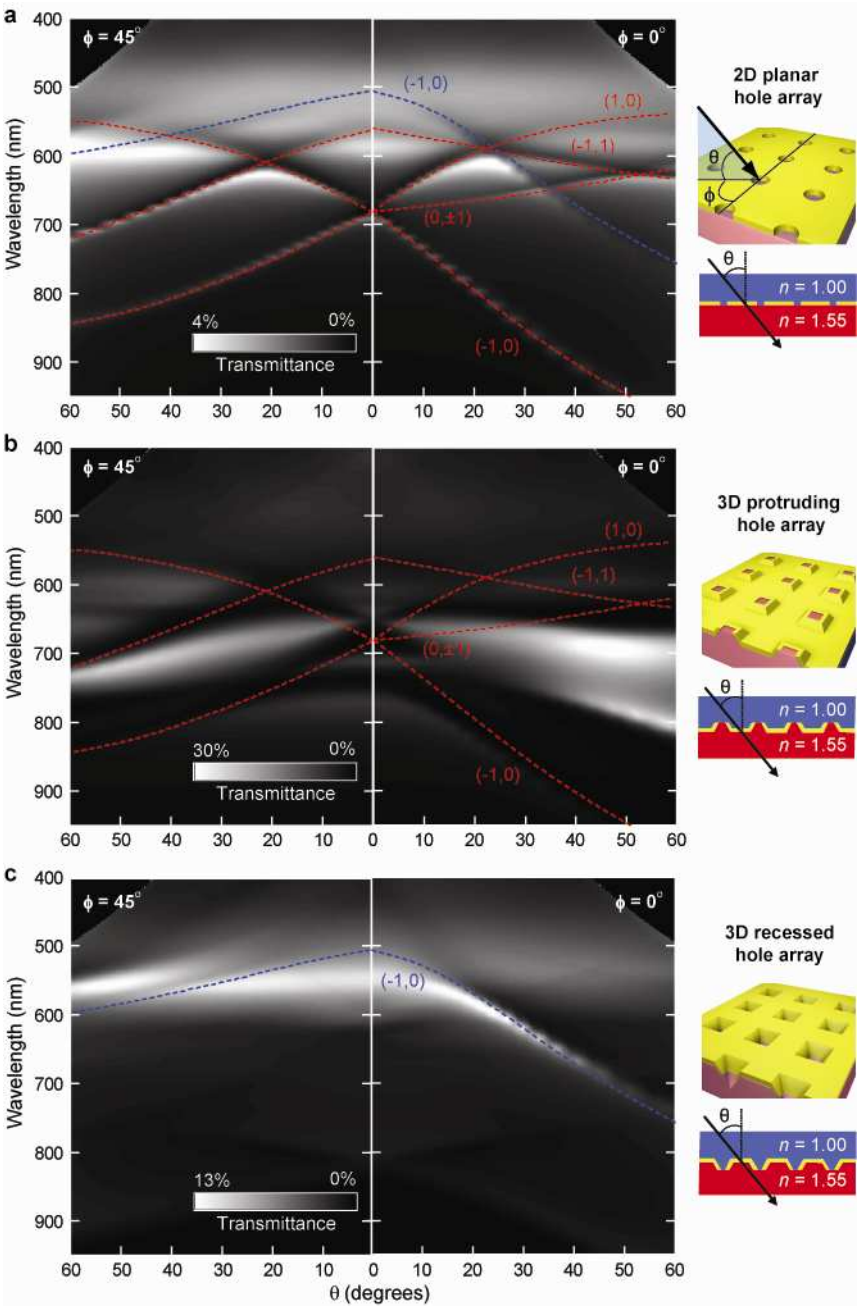

Figure S4. FDTD calculations confirm LSP-mediated transmission and SPP suppression. Angle-resolved optical transmission maps of **(a)** planar, **(b)** protruding and **(c)** recessed hole arrays calculated in air under *p*-polarized white light. Blue dashed curves denote SPP modes from the superstrate (air). Red dashed curves show SPP modes from the substrate (PU). θ is the incident angle of light, and ϕ is the azimuthal angle. All the important spectral features in Fig. 2 were reproduced by the FDTD calculations.

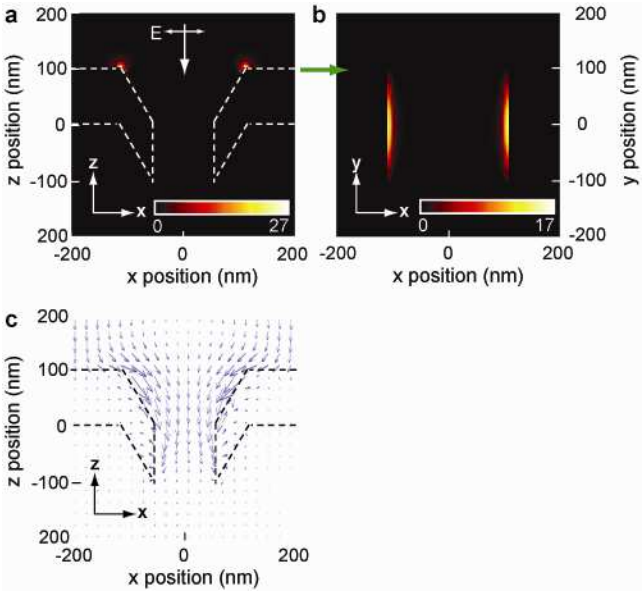

Figure S5. LSPs excited on 3D recessed hole arrays increase the energy flow inside the hole. FDTD calculations of $|E_z|^2$ at $\lambda = 530$ nm, $\theta = 0°$, $\phi = 0°$ (**IV** in Fig. 2) from the (**a**) side view and (**b**) top-down view. (**c**) Poynting vector map indicates that the energy flow is directly associated with the high transmission observed at **IV** in Fig. 2. The size of the arrows is proportional to the strength of energy flow.

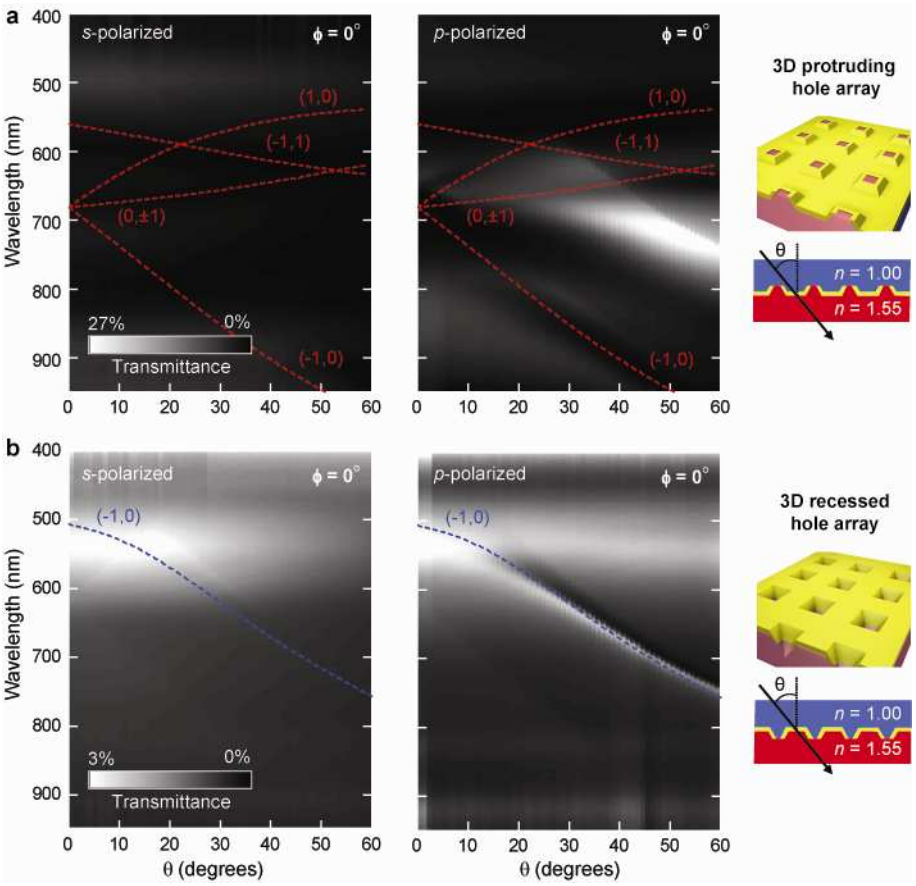

Figure S6. *s*-polarized light reveals different LSP-mediated optical transmission on 3D hole arrays. Optical transmission dispersion diagrams of **(a)** protruding and **(b)** recessed hole arrays in air under *s*-polarized and *p*-polarized white light. The symbols and curves are the same as those in Fig. 2. LSP-mediated transmission from 3D protruding and 3D recessed hole arrays show different dispersive properties under *s*-polarized light.

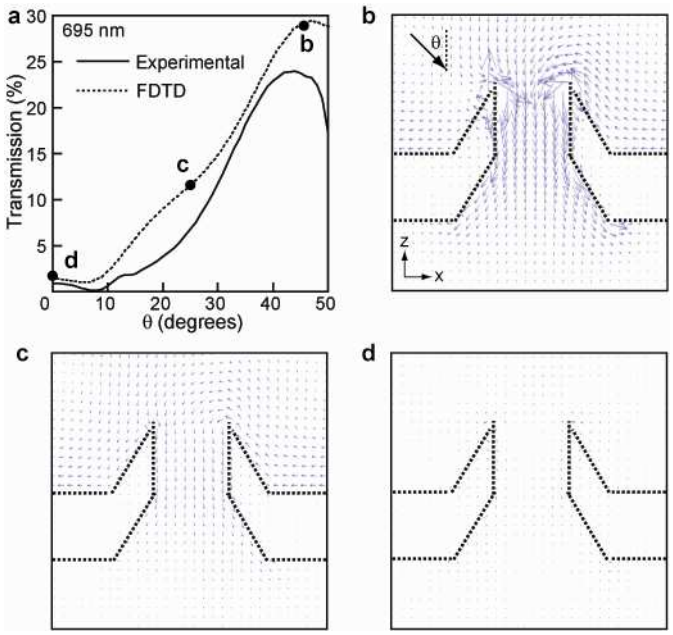

Figure S7. Localized fields on the edges of a 3D protruding hole under high incident angles increase energy flow inside the hole. (a) comparison of FDTD calculations and experiment at 695 nm at different angles of excitation. **(b)-(d)** maps of Poynting vectors on the protruding hole arrays with the excitation angles at θ = 45°, 25°, and 0°. The size of the arrows is proportional to the strength of energy flow.

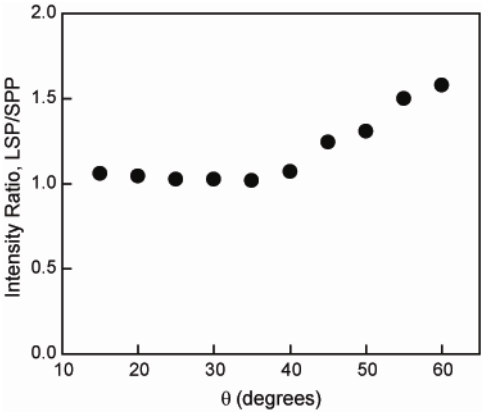

Figure S8. LSP excitations in 3D recessed hole arrays have higher transmission than SPPs. The intensity ratio of the LSP peak (around 530 nm) and the SPP (-1, 0) resonance of recessed hole arrays in Fig. 2c indicate that the LSP peak is always of higher intensity than the SPP (-1, 0) peak, especially at $\theta > 40°$.